Journal of Molecular Liquids 351 (2022) 118597

Contents lists available at ScienceDirect

Journal of Molecular Liquids

journal homepage: www.elsevier.com/locate/molliq

Controlling ambidextrous mirror symmetry breaking in photosensitive supramolecular polycatenars by alkyl-chain engineering

Mohamed Alaasar [a,b,*], Xiaoqian Cai [c], Felix Kraus [d], Michael Giese [d], Feng Liu [c], Carsten Tschierske [a,*]

[a] Institute of Chemistry, Martin Luther University Halle-Wittenberg, Kurt Mothes Str. 2, D-06120 Halle (Saale), Germany
[b] Department of Chemistry, Faculty of Science, Cairo University, Giza, Egypt
[c] State Key Laboratory for Mechanical Behavior of Materials, Shaanxi International Research Center for Soft Matter, Xi'an Jiaotong University, Xi'an 710049, PR China
[d] Institute of Organic Chemistry, University Duisburg-Essen, Universitätsstraße 7, 45141 Essen, Germany

ARTICLE INFO

Article history:
Received 2 December 2021
Revised 17 January 2022
Accepted 19 January 2022
Available online 1 February 2022

Keywords:
Polycatenar liquid crystals
Hydrogen bonding
Azobenzenes
Helical self-assembly
Cubic phases
Mirror symmetry breaking
Photo switching

ABSTRACT

Liquid crystalline (LC) photo sensitive materials capable of forming mirror-symmetry broken mesophases are of great interest to produce nano-structured materials for optical and photonic applications. Herein we report how mirror-symmetry breaking could be controlled in photo sensitive supramolecular polycatenars by alkyl chain engineering. For this purpose, three new series of supramolecular photoswitchable multi-chain complexes (polycatenars) formed by intermolecular hydrogen bonding interaction between azopyridines with one variable terminal chain as the proton-acceptors and Y-shaped or taper shaped benzoic acids having either two or three terminal chains as the hydrogen bond-donors were synthesized. The LC self-assembly of these supramolecules was characterized by differential scanning calorimetry (DSC), polarized optical microscopy (POM) and X-ray diffraction (XRD). Depending on the number and length of terminal chains spontaneously chiral isotropic liquid ($Iso_l^{[*]}$) as well as two different types of three dimensional (3D) bicontinous cubic phases are observed, which are either chiral ($Cub_{bi}^{[*]}/I23$) or achiral ($Cub_{bi}/Ia3d$). Moreover, UV light irradiation leads to the first fast and reversible photoinduced transformation between chiral and achiral 3D cubic phases as well as between a chiral crystalline and a chiral cubic liquid crystalline phase.

1. Introduction

Spontaneous mirror symmetry breaking in achiral liquid crystalline (LC) compounds is of special interest as it opens the door for providing an efficient way to produce chiral materials, thus being important from a scientific point of view, as well as for applications in functional materials [1–3]. Spontaneous ambidextrous chirality in LCs could be indicated by the observation of chiral conglomerates, which were found in mesophases formed by different classes of LCs. For example, bent-core LCs can form chiral domains in the optically isotropic dark-conglomerate (DC) phases, as well as in the fluid birefringent nematic (N) and SmC phases [4–14]. Another example is the chiral fluid twist bend nematic phases (N_{TB}) formed by bent dimesogens [15,16]. Non-covalent interactions, such as hydrogen bonding, has been applied as a very successful way to produce nanostructured functional LCs [17–19]. Intermolecular interactions either hydrogen or halogen-bonding between complementary components, which are in most cases non-mesomorphic, produce LCs with lamellar or columnar phases [20–24]. Inducing LC phases by hydrogen bond formation is known for dimers formed by 4-alkyl(oxy)benzoic acids, cyclohexane carboxylic acids or between benzoic acids and pyridine moieties [25–27]. More examples of LC materials with complex superstructures were also constructed by hydrogen-bond formation [28–33]. One of the interesting LC phases designed by H-bonding is the bicontinuous cubic phase (Cub_{bi}) phase. The dimers formed by intermolecular H-bond formation between 4′-*n*-alkoxy-3′-nitrobi phenyl-4-carboxylic acid molecules (ANBCs) represent the first examples of LCs exhibiting Cub_{bi} phases [34,35]. Later, hetero mixtures of ANBCs with 3,5-dialkoxybenzoic acids [36–38], and 2,4-diaminotriazines [39] were also found to form Cub_{bi} phases. Cub_{bi} phases are three dimensional (3D) LCs phases, representing interwoven networks of branched columns (Fig. 1**b,c**) characterized by their isotropic appearance under crossed polarizers and are very interesting from applications point of view by providing fast charge transport due to their 3D network structures [40–44].

* Corresponding author at: Institute of Chemistry, Martin Luther University Halle-Wittenberg, Kurt Mothes Str. 2, D-06120 Halle (Saale), Germany.
E-mail addresses: mohamed.alaasar@chemie.uni-halle.de (M. Alaasar), carsten.tschierske@chemie.uni-halle.de (C. Tschierske).

https://doi.org/10.1016/j.molliq.2022.118597
0167-7322/

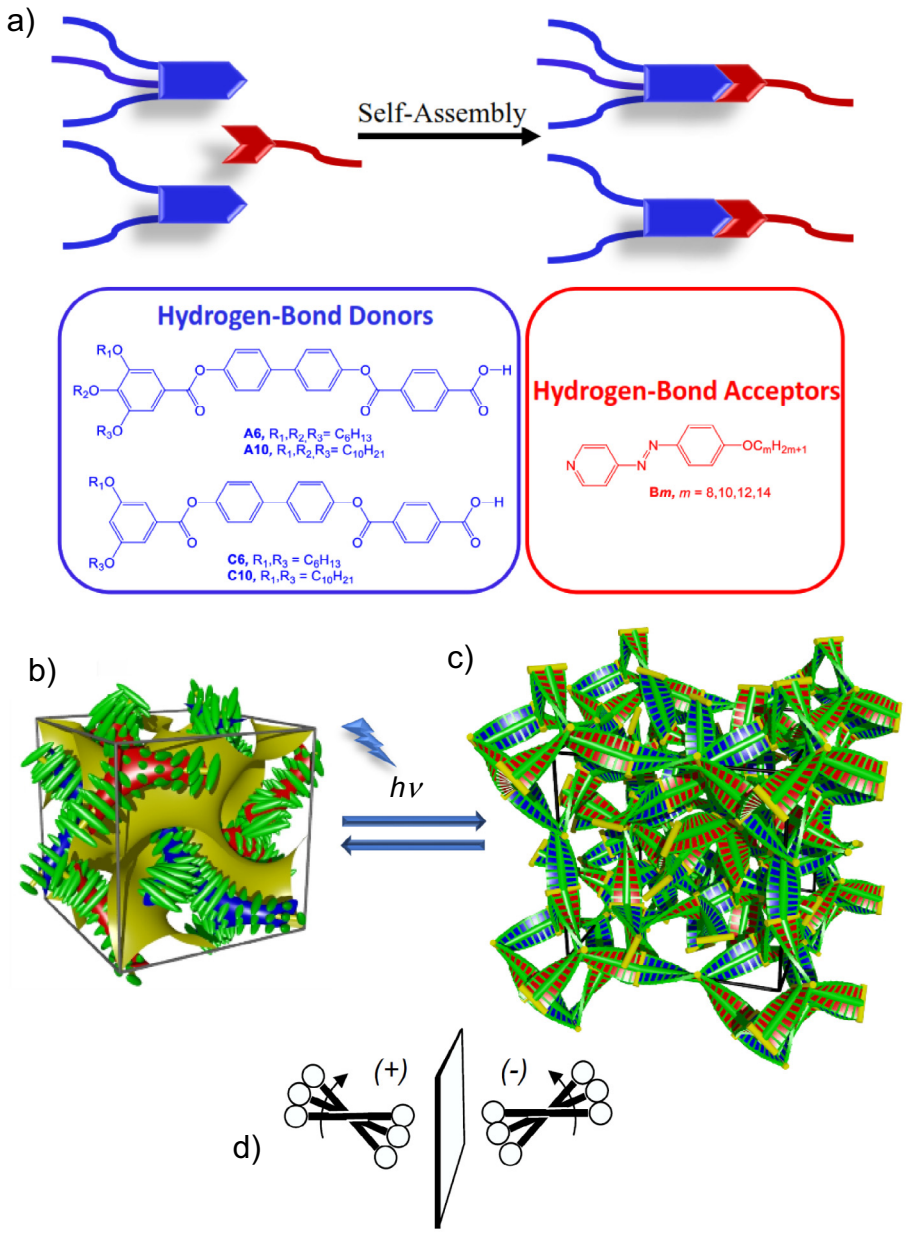

Fig. 1. (a) Schematic representation for the hydrogen-bond donors and acceptors yielding photoswitchable aggregates. (b) The double-gyroid achiral bicontinuous $Ia\bar{3}d$ phase having two networks with opposite chirality (red and blue) [47]. (c) The model proposed for the ambidextrous chiral $I23$ phase with three continuous networks [54]. (d) The development of the helical twist by the clashing of end groups attached to rod-like cores in the networks. (b) and (c) were reproduced from Refs. [46,49], by permission from Wiley-VCH and RSC, respectively.

Alkyl chain engineering has been used in the recent decades for the induction of Cub_{bi} phases by connecting more than only one alkyl chain to the ends of extended rod-like aromatic-core units i.e. polycatenar molecules and supramolecular aggregates [45,46]. By adjusting the volume, length and mode of distribution of the alkyl chains along the hydrogen bonded polyaromatic rods their self-assembly is modified by softening their hard-core interactions and by modification of the interfacial curvature between the nano-segregated aggregates of the rods and the surrounding chains. As the formation of mirror-symmetry broken liquid and LC phases is associated with network formation, a fine tuning of the lipophilic chains is often used to achieve the required degree of intermaterials interface curvature. Wide ranges of Cub_{bi} phases were found to be formed by taper shaped polycatenars in which the terminal alkyl chains are distributed non-symmetrically at both ends of the aromatic core [47–53]. Moreover, mirror symmetry breaking was observed in the triple network Cub_{bi} phases with space group $I23$ ($Cub_{bi}^{[*]}/I23$, Fig. 1c)[47,49–51,54] as well as in some cases in isotropic liquids assigned as $Iso_1^{[*]}$ phases [48]. In addition to the chiral $Cub_{bi}^{[*]}/I23$ phase, the achiral gyroid double network Cub_{bi} phase ($Ia\bar{3}d$, Fig. 1b) was also formed by polycatenars [40]. As shown in Fig. 1d, chirality arises from the helical packing of the crowded rod-like molecules with their long axes perpendicular to the local network direction. In addition, by alkyl chain engineering the twist angle between the rods is modified, which can be used to switch the space group of the cubic lattice between Iad and $I23$ [49,50]. The $Cub_{bi}/Ia\bar{3}d$ phase is achiral because of the opposite helix sense in the two enantiomorphic networks forming this phase cancels each other (thus forming a *meso-*

structure). In the *I*23 phase there are three networks and the overall chirality cannot be canceled leading to ambidextrous mirror symmetry breaking with chiral conglomerate formation [40,54].

The introduction of a photo switchable chromophore such as an azobenzene unit in the chemical structure yields light-responsive functional LCs because of the fast and reversible *trans–cis* photoisomerization upon light irradiation [55–65]. Photo switchable LCs phases are of special interest as their optical properties could be manipulated with light and therefore could be exploited for optoelectronic, tuneable photonics, and sensing devices [66–71]. Optical switching between lamellar and cubic phases was successively achieved and reported by Kutsumizu et al. [72,73]. The first examples of supramolecular photoesensitive polycatenar LCs designed by either hydrogen-bonding [74]or halogen-bonding supramolecular [75] were reported by our research group. The hydrogen-bonded polycatenars **A6/B*m*** (Fig. 1a) exhibit chirality synchronization in the $Cub_{bi}^{[*]}$/*I*23 phases as well as in the $Iso_{I}^{[*]}$ phase formed by the shortest homologue [74]. Very recently, the effect of aromatic core fluorination on the chiral network formation of **A6/B*m*** systems was investigated in detail [76]. As noted above the size and shape of the core as well as the length of the terminal chains are important factors which control the physical properties of LCs [77–80].

Herein, we use alkyl chain engineering in designing new LCs aiming to control the type of Cub_{bi} phases as well as network formation in the isotropic liquids exhibited by hydrogen-bonded supramolecular LCs systems (Fig. 1a). For this purpose, three new series of supramolecular polycatenars were designed and synthesized (**A10/B*m***, **C6/B*m*** and **C10/B*m***, see Scheme 1). The first type of these supramolecular polycatenars (**A10/B*m***) is formed by intermolecular H-bond formation between a taper-shaped triple chain benzoic acid derivative (**A10**) and azopyridine derivatives (**B*m***) terminated with one alkoxy chain, while the other two types (**C6/B*m*** and **C10/B*m***) are formed between the same azopyridine derivatives **B*m*** and double chain Y-shaped benzoic acid derivatives (**C6** and **C10**). Depending on the number and length of the terminal alkyl chains of the benzoic acid derivatives, these supramolecular dimers show a series of chiral and achiral Cub_{bi} phases, mirror-symmetry broken isotropic liquids ($Iso_{I}^{[*]}$) and columnar (Col) mesophases. Moreover, the first fast and reversible photoinduced transformation between chiral and achiral cubic phases was successfully achieved. with these new supramolecules.

2. Experimental

2.1. Synthesis

The synthesis of the new H-bonded supramolecules (**A10/B*m***, **C6/B*m*** and **C10/B*m***) is shown in Scheme 1. The proton acceptors 4-(4-alkoxyphenylazo)pyridine **B*m*** were synthesized as described before [60,81], while the synthesis details of the benzoic acid derivatives **A10**, **C6** and **C10**, as well as for the final supramolecules are given in the supporting information (SI). Homogenous melting and stable LC mesophases were observed for all supramolecules (Table 1 and Table 2).

2.2. Characterization

The formation of hydrogen-bonded 1:1 complexes between the 4-phenylazopyridines **B*m*** and the benzoic acid **A/6** was discussed and proven in previous work by IR spectroscopy and by the absence of DSC peaks corresponding to the transitions of the individual components [76]. Likewise, the formation of the supramolecules between the complementary components **A*n*** and **B*m*** was confirmed by the transition temperatures of the 1:1 complexes **A*n*:B*m* = A*n*/B*m*** (Table 1), which are distinct from the values of individual components as confirmed by differential scanning calorimetry (DSC) and polarized optical microscopy (POM). In the DSC curves all supramolecules do not show any transition of the pure azopyridine dervatives nor of the pure acids (see Figs. S8-S12), and only transition peaks of the newly formed hydrogen-bonded supramolecues could be observed (see Fig. 3).

POM was performed using a Mettler FP-82 HT hot stage and control unit in conjunction with a Nikon Optiphot-2 polarizing microscope. The associated enthalpies were obtained from DSC-thermograms which were recorded on a Perkin-Elmer DSC-7, heating and cooling rate: 10 K min^{-1}.

X-ray diffraction (XRD) was performed for selected complexes (**A10/B8, B10** and **B14**, **C10/B8, B14**, and **C6/B14**, see Tables S3-S18 and Figs. S11-S20). High-resolution small angle powder diffraction experiments were recorded on Beamlines BL16B1 at Shanghai Synchrotron Radiation Facility (SSRF). Samples were held in evacuated 1 mm capillaries. A modified Linkam hot stage with thermal stability within 0.2 °C was used, with a hole for the capillary drilled through the silver heating block and mica windows attached to it on each side. θ-calibration and linearization were verified using several orders of layer reflections from silver behenate and a series of *n*-alkanes. A Pilatus detector was used for SAXS. The phase transitions of all complexes are collated in Table 1 and Table 2.

Photo switching experiments were performed using Hönle bluepoint LED eco with 365 nm head with maximum output of 14 W/cm^2.

3. Results and discussion

3.1. Self-assembly of the four-chain supramolecules An/Bm

Before discussing the LC behaviour of the hydrogen-bonded complexes, it should be noted that all of the pyridine-based compounds **B*m*** are non-mesomorphic i.e. crystalline solids with relatively low melting temperatures (see **Table S1**, Fig. S11,12), while the hydrogen-bond donor i.e. the benzoic acid derivative **A6** with three hexyloxy chains is a hexagonal columnar LC (Col_{hex}, a_{hex} = 5.4-nm) with a high clearing temperature at ~246 °C [74]. Because of the very similar structure of the acid **A6** compared to **A10** with the three hexyloxy chains replaced by three longer decyloxy chains and based on the observed optical textures (see Fig. S7a), the acid **A10** is also considered to exhibit a Col_{hex} phase between 128 and 230 °C (see Table S2 and Fig. S8). The formation of this phase is a result of dimer formation between the free carboxylic groups leading to hexacatenar supramolecules with six symmetrically distributed terminal chains [74]. Upon H-bond formation with the azopyridine derivatives having only one alkyoxy chain different phase sequences of cubic network phases, in some cases accompanied by columnar mesophases, are observed for all resulting 1:1 complexes **A*n*/B*m*** (see Table 1 **and** Fig. 2).

The phase behaviour of the supramolecules **A6/B*m*** was discussed in detail in our previous communication [74]. However for comparison reason the transition temperatures of **A6/B*m*** as well as for the newly reported aggregates **A10/B*m*** are collected in Table 1 and represented graphically in Fig. 2.

The complex formation between **A*n*** and **B*m*** leads to the suppression or reduction of the Col_{hex} phase range exhibited by the pure acids **A*n*** and the induction of new LCs phases. This means that the hexacatenars formed by hydrogen bonding between the benzoic acids **A*n*** are replaced by non-symmetric tetracatenars **A*n*/B*m*** involving benzoic acid pyridine H-bonding and having only four terminal chains distributed in 3 + 1 fashion at both ends of the extended aromatic core. This alkyl chain substitution pattern is

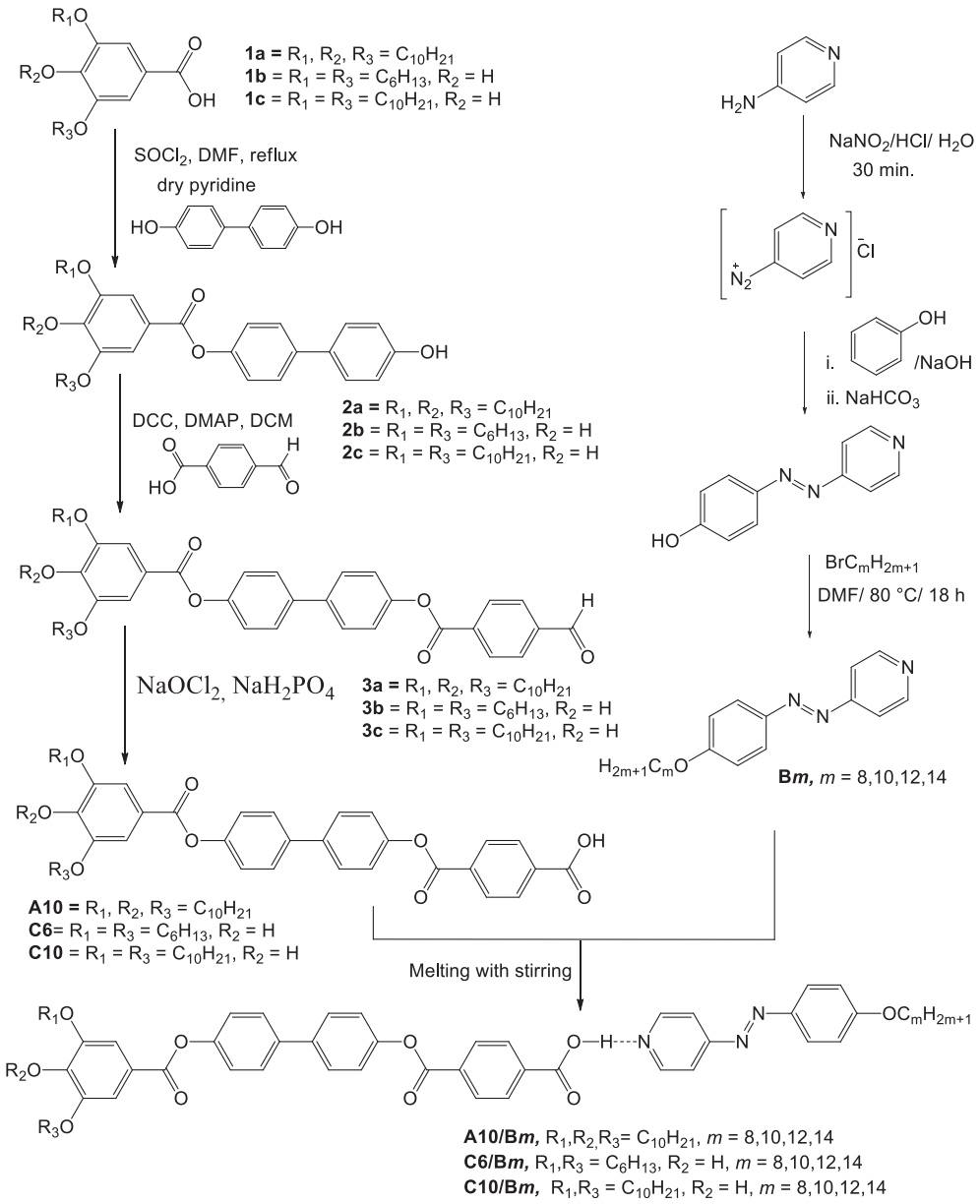

Scheme 1. Synthesis of the azopyridines **B*m***, the benzoic acids **A10**, **C6**, **C10** and the hydrogen-bonded 1:1 complexes (**A10/B*m***, **C6/B*m*** and **C10/B*m***).

known to support the formation of Cub_{bi} phases as well as $Iso_1^{[*]}$ phases due to the smaller average number of alkyl chains which reduces the interface curvature and leads to a transition from non-branched columns in the Col_{hex} phase to three-way branched networks in the Cub_{bi} phases [60,62].

For all supramolecules **A10/B*m***, only the phase transitions between LC phases as well as the melting and crystallization are visible in the DSC curves. This is not affected by the used heating/-cooling rates (5, 10 and 20 K min^{-1}). However, all phase transitions could be optically observed under POM (Fig. 2 and Table 1). In all LC phases exhibited by these supramolecules, the WAXS scattering is completely diffuse with a maximum around 0.45 nm confirming the existence of LC phases without fixed positions of the individual molecules (Figures S19-S21).

As can be seen from Table 1 and Fig. 2 the shortest supramolecule **A10/B8** of the series **A10/B*m*** exhibits two different types of LC phases. Upon heating **A10/B8** from the birefringent crystalline solid a highly viscous and optically isotropic mesophase is observed, which remains over ~20 K. Under slightly uncrossed polarizers this isotropic phase does not show chiral domains, indicating the presence of an achiral cubic phase (Fig. 4**a,b**). On further heating the viscosity of the sample does not change but chiral domains, (assigned with $^{[*]}$) could be observed between not fully crossed polarizers in the temperature range of this second cubic phase till the transition to the highly fluid isotropic liquid state which is achiral again (Fig. 4c,d).

The chiral conglomerate indicates a chiral $Cub_{bi}^{[*]}$ phase [47]. On cooling **A10/B8** from the isotropic liquid the achiral Cub_{bi} phase is observed for a short range ~5 K, while the range of the chiral $Cub_{bi}^{[*]}$ phase is increased to ~96 K compared to ~67 K on heating. It is also interesting that the formed weakly birefringent crystalline phase on cooling the $Cub_{bi}^{[*]}$ phase is also chiral, having the chiral domains at the same positions as observed for the $Cub_{bi}^{[*]}$ phase. This indicates that the chirality information of the $Cub_{bi}^{[*]}$ mesophase is transferred to the crystalline state resulting in the formation of a mirror-symmetry broken crystalline phase ($Cr^{[*]}$, Fig. 4e,f). No such $Cr^{[*]}$ phase is observed for the homologous complexes **A10/*m*** with larger *m*.

Table 1
Phase transition temperatures (T/°C), mesophase types, and transition enthalpies [ΔH/kJ mol^{-1}] of the supramolecular complexes **An/Bm**.[a]

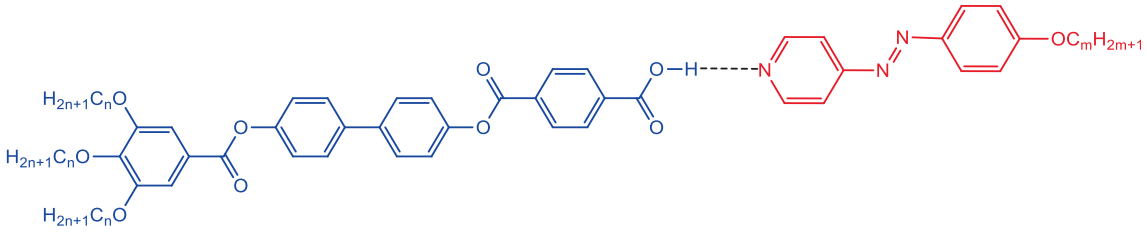

Complex	n	m	Phase transition
A6/B8[74]	6	8	**H:** Cr 124 [30.3] ~ 187 [0.1] Cub$^{[}_{bi}{}^{*]}$/*I*23 196 [0.1] Iso$^{[}_{I}{}^{*]}$ 200 [0.1] Iso **C:** Iso 190 [−0.1] Iso$^{[}_{I}{}^{*]}$ 183 [−0.1] Cub$^{[}_{bi}{}^{*]}$/*I*23 75 [−24.8] Cr$^{[*]}$
A6/B10[74]	6	10	**H:** Cr$_1$ 115 [12.2] Cr$_2$ 128 [45.4] Cub$^{[}_{bi}{}^{*]}$/*I*23 201 [0.9] Iso **C:** Iso 195 [−0.8] Cub$^{[}_{bi}{}^{*]}$/*I*23 75 [−38.8] Cr
A6/B12[74]	6	12	**H:** Cr 123 [54.5] Cub$^{[}_{bi}{}^{*]}$/*I*23 191 [1.4] Iso **C:** Iso 182 [−1.9] Cub$^{[}_{bi}{}^{*]}$/*I*23 87 [−45.4] Cr
A6/B14[74]	6	14	**H:** Cr 92 [31.4] Cub$^{[}_{bi}{}^{*]}$/*I*23 184 [1.9] Iso **C:** Iso 177 [−2.1] Cub$^{[}_{bi}{}^{*]}$/*I*23 < 20 Cr
A10/B8	10	8	**H:** Cr 80 [31.5] Cub$_{bi}$/*Ia* $\bar{3}$ *d* 100 [−] Cub$^{[}_{bi}{}^{*]}$/*I*23 167 [−] Iso **C:** Iso 159 [−0.4] Cub$_{bi}$/*Ia* $\bar{3}$ *d* 155 [−] Cub$^{[}_{bi}{}^{*]}$/*I*23 59 [−37.7] Cr$^{[*]}$
A10/B10	10	10	**H:** Cr 100 [40.4] Cub$^{[}_{bi}{}^{*]}$/*I*23 160 [−] Cub$_{bi}$/*Ia* $\bar{3}$ *d* 167 [−] Iso **C:** Iso 160 [−] Col$_{hex}$ 147 [−0.5] Cub$^{[}_{bi}{}^{*]}$/*I*23 60 [−38.4] Cr
A10/B12	10	12	**H:** Cr 98 [37.9] Cub$^{[}_{bi}{}^{*]}$/*I*23 147 [0.5] Cub$_{bi}$/*Ia* $\bar{3}$ *d* 154 [−] Col$_{hex}$ 172 [−] Iso **C:** Iso 171 [−] Col$_{hex}$ 133 [−] Cub$^{[}_{bi}{}^{*]}$/*I*23 47 [−34.4] Cr
A10/B14	10	14	**H:** Cr 69 [45.2] Cub$^{[}_{bi}{}^{*]}$/*I*23 141 [0.5] Cub$_{bi}$/*Ia* $\bar{3}$ *d* 159 [−] Col$_{hex}$ 175 [−] Iso **C:** Iso 173 [−] Col$_{hex}$ 114 [−0.4] Cub$^{[}_{bi}{}^{*]}$/*I*23 32 [−24.2] Cr

[a]Peak temperatures as determined from 2nd heating and 2nd cooling DSC scans with rate 10 K min^{-1}; abbreviations: Cr = crystalline solid; Cub$_{bi}$/*Ia*$\bar{3}$*d* = achiral cubic phase with *Ia*$\bar{3}$*d* lattice; Cub$^{[}_{bi}{}^{*]}$/*I*23 = chiral cubic phase with *I*23 lattice, forming a chiral conglomerate; Col$_{hex}$ = hexagonal columnar phase with *p*6*mm* lattice; Iso$^{[*]}$ = chiral isotropic conglomerate liquid; Iso = achiral isotropic liquid; for complete structural data, see Tables S6 and S19.

Table 2
Phase transition temperatures (T/°C), mesophase types, and transition enthalpies [ΔH/kJ mol^{-1}] of the supramolecular complexes **Cn/Bm**.[a]

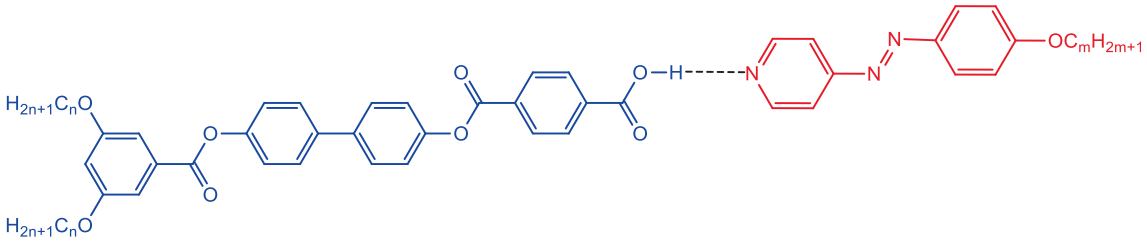

Complex	n	m	Phase transition
C6/B8	6	8	**H:** Cr 119 [35.5] Cub$_{bi}$/*Ia* $\bar{3}$ *d* 173 [0.2] Iso **C:** Iso 166 [−0.5] Cub$_{bi}$/*Ia* $\bar{3}$ *d* 90 [−33.0] Cr
C6/B10	6	10	**H:** Cr 127 [30.3] Cub$_{bi}$/*Ia* $\bar{3}$ *d* 157 [0.2] Iso **C:** Iso 139 [−0.2] Cub$_{bi}$/*Ia* $\bar{3}$ *d* 76 [−26.9] Cr
C6/B12	6	12	**H:** Cr 117 [44.7] Cub$_{bi}$/*Ia* $\bar{3}$ *d* 157 [0.3] Iso **C:** Iso 151 [−0.4] Cub$_{bi}$/*Ia* $\bar{3}$ *d* 71 [−41.0] Cr
C6/B14	6	14	**H:** Cr 99 [28.7] Cub$_{bi}$/*Ia* $\bar{3}$ *d* 157 [0.7] Iso **C:** Iso 151 [−0.9] Cub$_{bi}$/*Ia* $\bar{3}$ *d* 58 [−31.7] Cr
C10/B8	10	8	**H:** Cr 118 [42.3] Cub$_{bi}$/*Ia* $\bar{3}$ *d* 183 [2.0] Iso **C:** Iso 178 [−1.7] Cub$_{bi}$/*Ia* $\bar{3}$ *d* 111 [−14.5] Cr$_1$ 94 [−21.4] Cr$_2$
C10/B10	10	10	**H:** Cr$^{[*]}$ 103 [37.4] Cub$^{[}_{bi}{}^{*]}$/*I*23 178 [1.6] Iso **C:** Iso 176 [−0.1] Iso$^{[}_{I}{}^{*]}$ 167 [−0.7] Cub$^{[}_{bi}{}^{*]}$/*I*23 94 [−35.6] Cr$^{[*]}$
C10/B12	10	12	**H:** Cr$^{[*]}$ 108 [29.1] Cub$^{[}_{bi}{}^{*]}$/*I*23 183 [0.7] Iso$^{[}_{I}{}^{*]}$ 200 [0.3] Iso **C:** Iso 188 [−0.3] Iso$^{[}_{I}{}^{*]}$ 174 [−0.4] Cub$^{[}_{bi}{}^{*]}$/*I*23 90 [−27.5] Cr$^{[*]}$
C10/B14	10	14	**H:** Cr 103 [33.9] Cub/*Ia* $\bar{3}$ *d* 150 [−] Cub$^{[}_{bi}{}^{*]}$/*I*23 185 [2.1] Iso **C:** Iso 179 [−1.0] Col$_{hex}$ 173 [−0.4] Cub$^{[}_{bi}{}^{*]}$/*I*23 89 [−23.2] Cr

[a]Peak temperatures as determined from 2nd heating and 2nd cooling DSC scans with rate 10 K min^{-1}; for abbreviations see Table 1; for complete structural data, see Table S19.

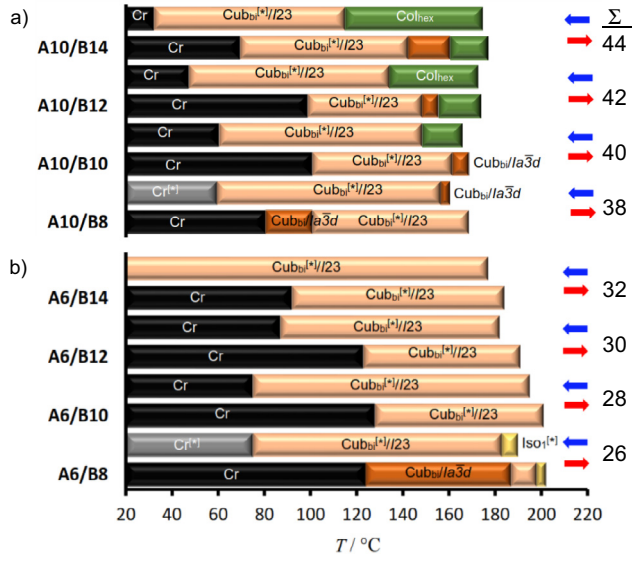

Fig. 2. Phase transitions of: (a) the new H-bonded supramolecules **A10**/**B*m*** and (b) the previously reported **A6**/**B*m*** supramolecules as observed by DSC and POM on heating (lower bars, red arrows) and on cooling (upper bars, blue arrows) with 10 K min^{-1}; Σ*n* is the total number of C-atoms in the lipophilic chains (3*n* + *m*).

To study both cubic phases in more detail, the supramolecule **A10/B8** was further investigated by X-ray diffraction with a synchrotron source (Fig. 5 and Tables S3-S5). Upon heating two intense diffraction peaks are observed at ~90 °C in the lower temperature achiral Cub$_{bi}$ phase which are indexed to (211) and (220) reflections known for a $Ia\bar{3}d$ lattice with a cubic lattice parameter of a_{cub} = 13.15 nm (Fig. 5a) confirming a double network gyroid cubic phase [40]. Moreover, the additional much smaller scatterings at higher θ-values fit also with the $Ia\bar{3}d$ space group. In the higher temperature chiral Cub$_{bi}$ phase the most intense peaks can be indexed as (321) and (400) reflections of a *I*23 lattice (Fig. 5b and Table S4) [76]. The lattice parameter of this chiral cubic phase is a_{cub} = 21.58 nm and thus 65 % larger than that in the $Ia\bar{3}d$ lattice (a_{cub} = 13.15 nm). The increased lattice parameter is in agreement with a transition from a double network to a triple network Cub$_{bi}$ phase [54]. The structures of the two different Cub$_{bi}$ phases was further confirmed by the reconstruction of electron density maps based on the obtained diffraction patterns, which show the double network structure of the $Ia\bar{3}d$ phase and the triple-network structure of the *I*23 phase (Fig. 5c,d).

Upon cooling **A10/B8** from the isotropic liquid, a small range of an achiral $Ia\bar{3}d$ phase appears before the chiral *I*23 phase, as indicated by the absence of any chiral conglomerate texture in the highly viscous and optically isotropic cubic phase. Additional support comes from SAXS investigation, showing the typical diffraction pattern of a cubic phase with $Ia\bar{3}d$ space group (Table S5). However, in this $Ia\bar{3}d$ phase the lattice parameter a_{cub} = 12.32 nm at 160 °C is significantly smaller than in the low temperature $Ia\bar{3}d$ phase observed at 90 °C on heating (a_{cub} = 13.15 nm, see Tables 1 and S6).

The next longer hydrogen-bonded supramolecule with *m* = 10, i.e. **A10/B10,** shows an inverse phase sequence Cub$_{bi}^{*}$/*I*23 → Cub$_{bi}$/$Ia\bar{3}d$ on heating (for XRD data, see Tables S7-S9 and Figs. S14). Moreover, on cooling from the isotropic liquid the achiral double network Cub$_{bi}$/$Ia\bar{3}d$ phase is completely replaced by a hexagonal columnar phase (Col$_{hex}$ with a_{hex} = 6.17 nm, see Fig. 6**b** and Table S9) followed by the chiral Cub$_{bi}^{*}$/*I*23 phase, which is retained till crystallization (see Table 1, Fig. 6**a**). For the longest supramolecules **A10/B12** and **A10/B14** phase sequences involving three different LC phases are observed on heating (Cub$_{bi}^{*}$/*I*23 → Cub$_{bi}$/$Ia\bar{3}d$ → Col$_{hex}$/*p*6*mm*) and in the cooling cycle the Cub$_{bi}$/$Ia\bar{3}d$ phase is completely removed while only the Col$_{hex}$/*p*6*mm* and Cub$_{bi}^{*}$/*I*23 phases are observed (see Fig. 2 and Table 1). The formation of the Col$_{hex}$/*p*6*mm* phase was not observed for any of the supramolecular complexes **A6/B*m*** with three shorter hexyloxy chains at the benzoic acid side, indicating that the formation of this columnar phase requires long alkyl chains. The reason for Col$_{hex}$ phase formation is that thermal alkyl chain expansion increases the aromatic-aliphatic interface curvature which then leads to the transition from branched columns in the Cub$_{bi}$ phases to non-branched columns in the Col$_{hex}$ phase.

Overall, in the series of H-bonded complexes **A*n*/B*m*** reported here, there are two distinct ranges for the $Ia\bar{3}d$ phase. Those of the compounds with a total number of C-atoms in the aliphatic chains Σ < 28 (Fig. 2b) and those with Σ > 32 (Fig. 2a). For **A10/B8** there are two $Ia\bar{3}d$ phases, one formed at low temperature on heating before the transition to *I*23 ($Ia\bar{3}d^{LT}$ phase), the other one at higher temperature and formed on cooling from the isotropic liquid state ($Ia\bar{3}d^{HT}$). For the higher homologs of the series **A10/**

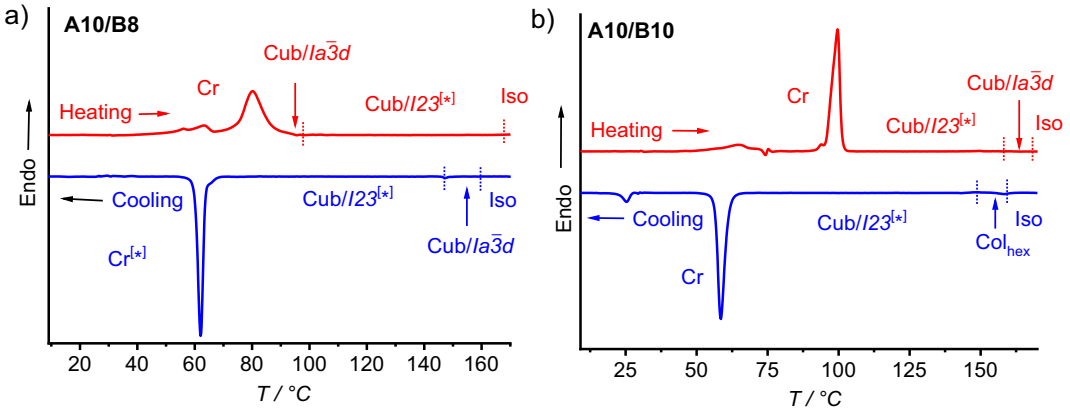

Fig. 3. DSC traces for the supramolecular complexes: (a) **A10/B8** and (b) **A10/B10** with heating and cooling rates of 10 K.min^{-1}; the DSCs of the individual components are shown in Figs. S19-S21.

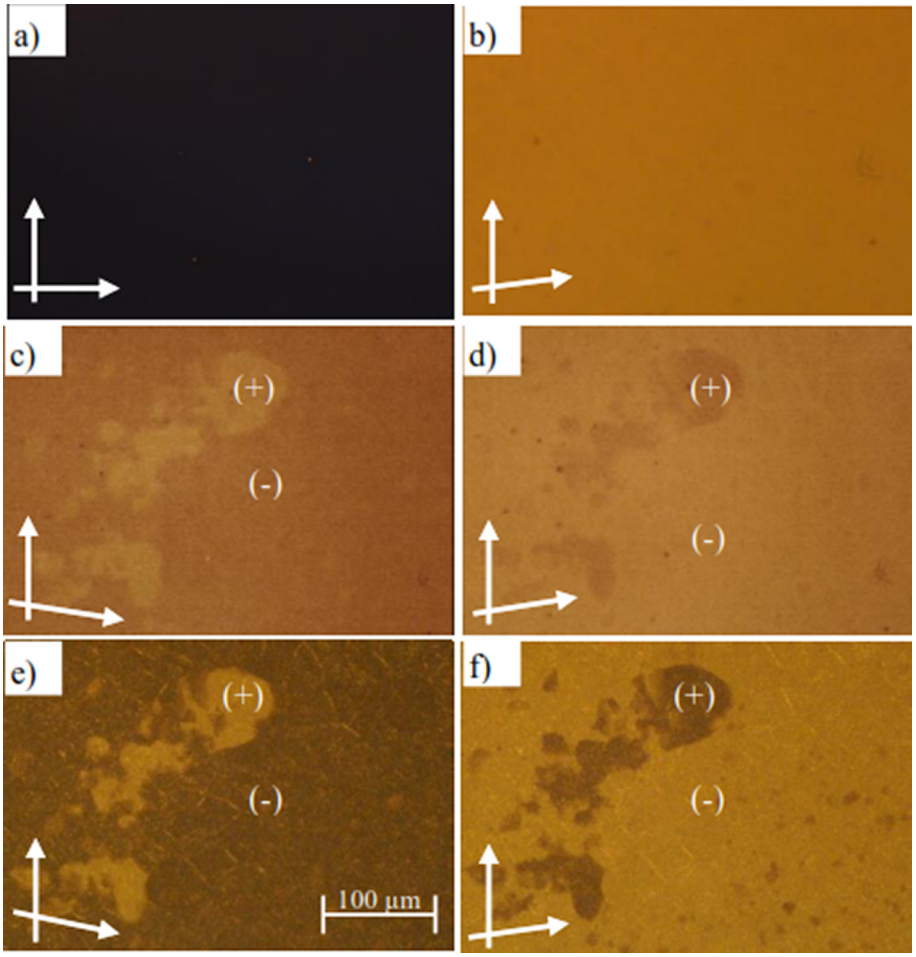

Fig. 4. Textures of the supramolecule **A10/B8** as observed on cooling in: (a) the achiral $Cub_{bi}/Ia\bar{3}d$ at T = 157 °C under crossed polarizers; (b) after rotating one polarizer from the crossed position by 15° in clockwise direction; (c,d) in $Cub_{bi}^{[*]}/I23$ at T = 120 °C after rotating one polarizer from the crossed position in clockwise or anticlockwise directions with the same angle showing dark and bright domains and in (e,f) in the chiral crystalline phase $Cr^{[*]}$.

B*n* with $m \geq 8$ there is no $Ia\bar{3}d^{L\ T}$ phase, only $Ia\bar{3}d^{HT}$. Moreover, it appears that there are even two distinct types of this $Ia\bar{3}d^{HT}$ phase, that of **A10/B8** occurring on cooling from the Iso phase has the smallest a_{cub} value (12.3 nm), whereas for compounds with m = 10,14 it occurs on heating above the $I23$ phase and has a significantly larger value a_{cub} of 13.5–13.6 nm (Fig. 2a). Moreover, all compounds with longer chains than **A10/B8** form a Col_{hex} phase and no $Ia\bar{3}d^{HT}$ phase on cooling, though $Ia\bar{3}d^{HT}$ is observed on heating above the chiral $I23$ phase, followed by Col_{hex} on further heating. This could be understood if the $Ia\bar{3}d^{HT}$ phase of **A10/B8**, formed on cooling from the achiral isotropic liquid would be achiral due to the absence of any long-range helical twist along the networks. In this case the lattice parameter is exclusively determined by the molecular parameters and volume effects (see Table S6 in SI) and not by any helix pitch length, and therefore can be very different from those of the *Iad* phases with helical structure [40,47]. In contrast, the $Ia\bar{3}d^{HT}$ phases of compounds **A10/B10** - **A10/B14** developing from the chiral $I23$ phase on heating and showing larger and very similar lattice parameters are likely to represent helical network phases, i.e. the helical organization present in the networks of the $I23$ phase is retained at the transition to $Ia\bar{3}d^{HT}$. Only at the transition to Col_{hex} the long-range helical pitch is lost after removal of the network junctions. However, in order to certainly distinguish between helical and non-helical subtypes of the $Cub_{bi}/Ia\bar{3}d^{HT}$ phase, additional resonant soft X-ray scattering (RSoXS) investigations would be required [40,82].

It should be noted that for the complexes **A10/B*m*** no mirror-symmetry broken isotropic liquid phase ($Iso_{]}^{[*]}$), like that one recorded for the shortest supramolecule in the **A6/B*m*** series is observed (see Table 1 and Fig. 2). This means that $Iso_{]}^{[*]}$ phase formation requires small chain volumes and is anyhow associated with the $Ia\bar{3}d \rightarrow I23$ transition of the complexes with relatively short chains.

3.2. Liquid crystal self-assembly of the Y-shaped three-chain supramolecules Cn/Bm

In order to avoid the formation of Col_{hex} phases and to further modify the LC behaviour in these supramolecular aggregates by alkyl chain engineering, Y-shaped benzoic acid derivatives **C*n*** with smaller total chain volume were used as the proton donors (see Fig. 1 and Scheme 1). The formed tricatenars **C*n*/B*m*** have one less alkyl chain; namely the middle chain at 4-position of the benzoic acids **C*n*** is removed compared to the related analogues **A*n*** (see Fig. 7 and Table 2). This modification increases the melting temperatures of all **C*n*/B*m*** complexes compared to the complexes **A*n*/B*m*** and retains the 3D cubic phases formed by the **A*n*/B*m*** supramolecules. However, for the aggregates **C6/B*m*** having shorter alkyl chains at the benzoic acid side exclusively the achiral $Cub_{bi}/Ia\bar{3}d$

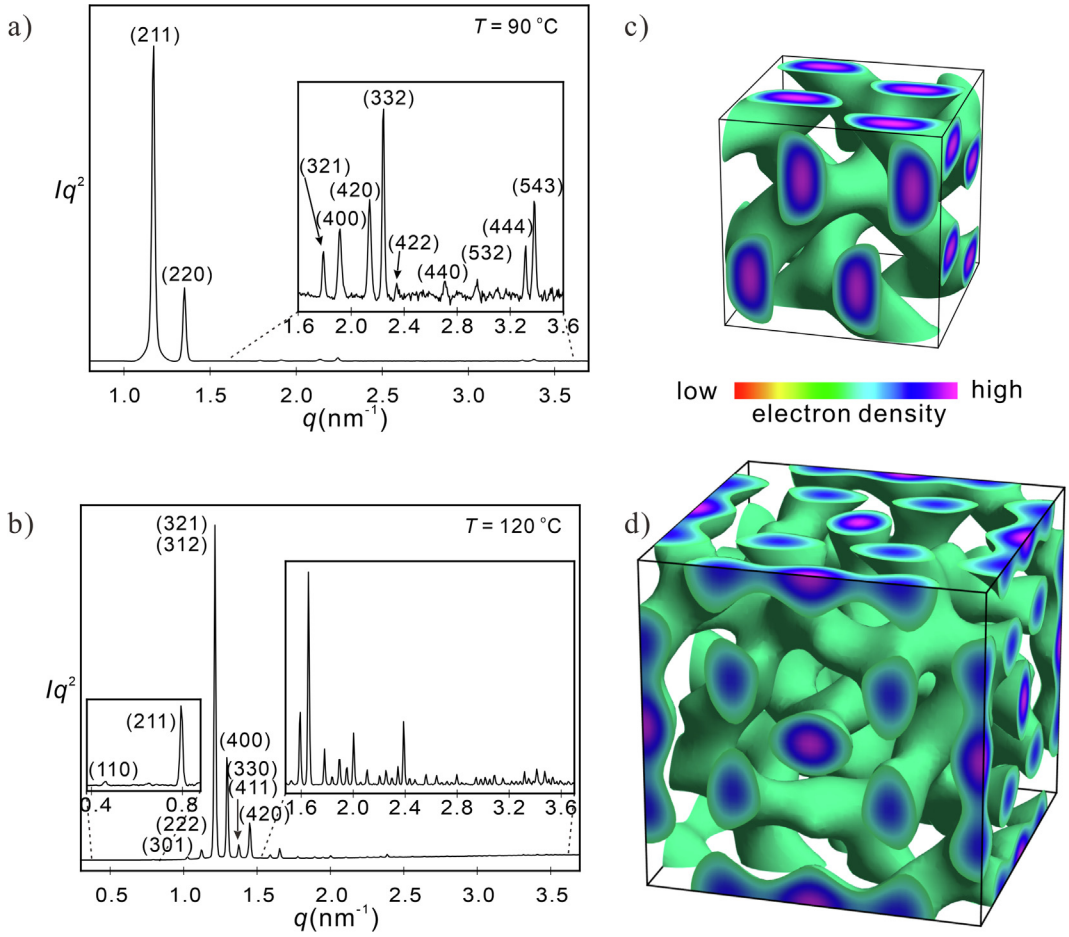

Fig. 5. (a,b) SAXS diffractograms of **A10/B8** on heating: a) in the $Cub_{bi}/Ia\bar{3}d$ phase at 90 °C (a_{cub} = 13.15 nm) and b) in the $Cub_{bi}^{[*]}/I23$ phase at 120 °C (a_{cub} = 21.58 nm); (c, d) electron density maps of (c) the $Ia\bar{3}d$ phase and (d) the $I23$ phase reconstructed from the diffraction data in (a, b); for numerical XRD data, see Tables S3, S4 in SI.

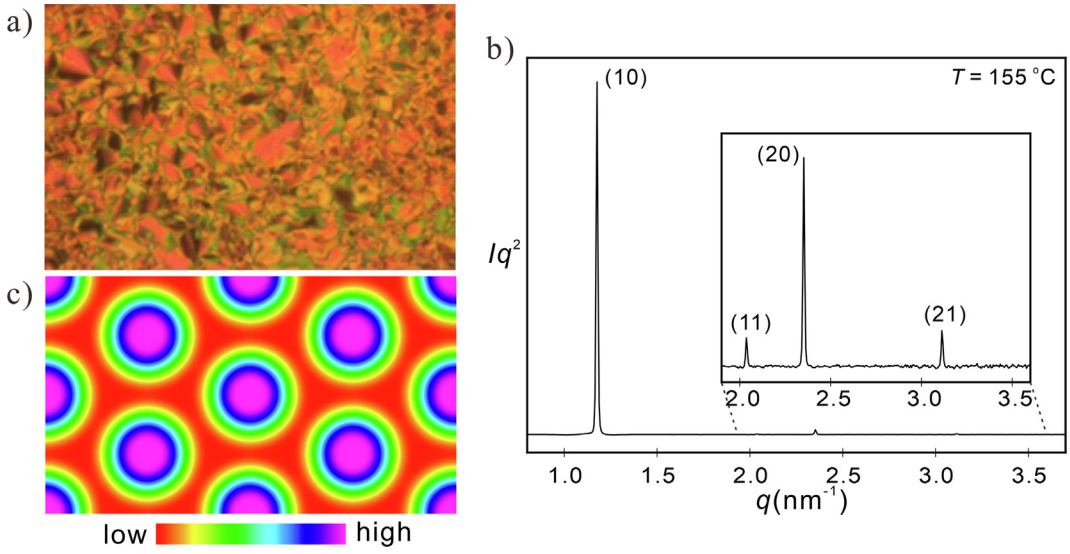

Fig. 6. (a) Texture of the supramolecule **A10/B10** as observed on cooling in the $Col_{hex}/p6mm$ phase at T = 155 °C; (b) SAXS diffractogram at 155 °C upon cooling of **A10/B10** (**a_{hex} = 6.17 nm**); (c) reconstructed electron density map for $Col_{hex}/p6mm$ phase of **A10/B10**.

phase is observed (see Fig. 7, for XRD data see **Fig. S16** and **Table S13, S14**).

Increasing the number of carbon atoms in the terminal chains of the proton donor **C*n*** to n = 10 instead of 6 results in the formation of **C10/B*m*** supramolecules. In this case for the shortest derivative **C10/B8** the achiral $Cub_{bi}/Ia\bar{3}d$ phase (see **Fig. S17**) is retained like in **C6/B8**. On chain elongation mirror-symmetry breaking is induced in the crystalline state ($Cr^{[*]}$) as well as in the cubic phase

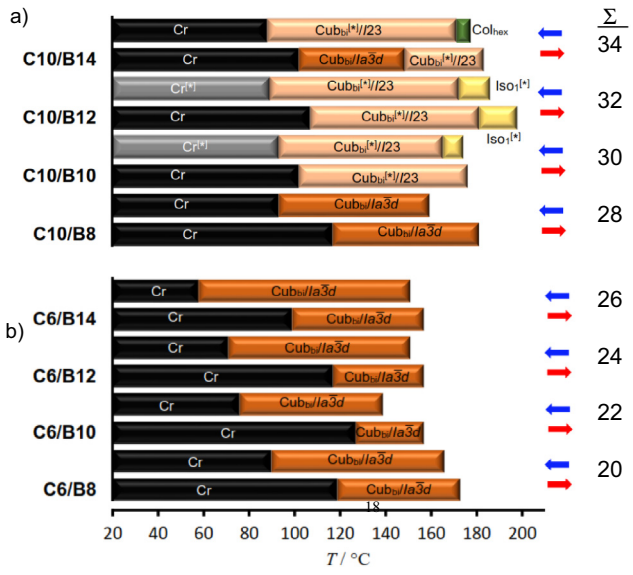

Fig. 7. Phase transitions of the new H-bonded supramolecules: (a) **C10**/**B*m*** and (b) **C6**/**B*m*** as observed by DSC and POM on heating (lower bars, red arrows) and on cooling (upper bars, blue arrows) with 10 K min^{-1}. Σ is the total number of C-atoms in the lipophilic chains (*2n* + *m*).

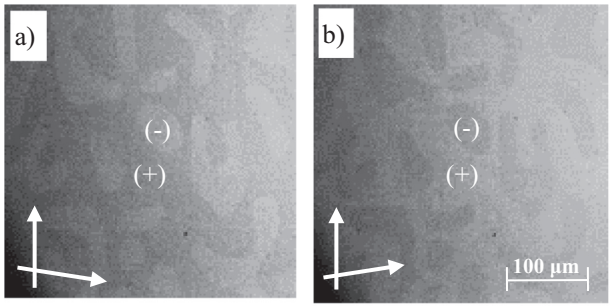

Fig. 8. Textures of the supramolecule **C10/B10** as observed on cooling in the chiral Iso$_1^{[*]}$ phase at *T* = 170 °C: (a) after rotating one polarizer from the crossed position in clockwise direction and (b) in anticlockwise direction showing dark and bright domains.

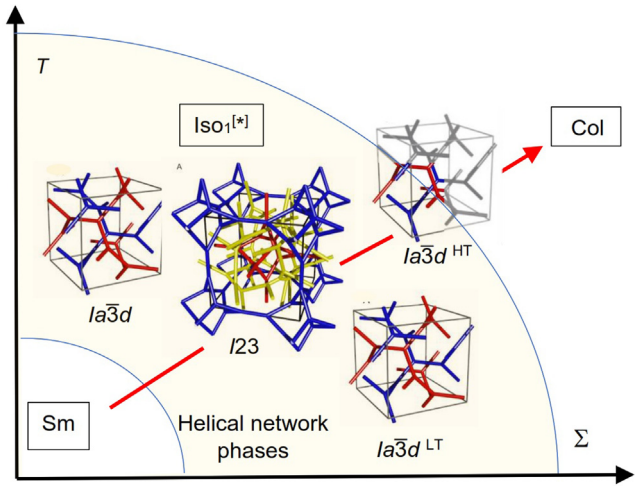

Fig. 9. Development of the different network phases depending on chain volume and temperature.

and even after transition to the isotropic liquid as observed for both middle chain homologues **C10/B10** and **C10/B12**. Chirality of these phases was confirmed by the dark and bright domains observed in the cooling cycles in the highly fluid isotropic liquid under slightly uncrossed polarizers (Fig. 8**a, b**). This indicates a chiral isotropic liquid, composed of a conglomerate of chiral domains (Iso$_1^{[*]}$), which is not formed by any of the **A10/B*m*** aggregates.

The Iso$_1^{[*]}$ phase of **C10/B10** appears only on cooling as metastable phase and as enantiotropic one for **C10/B12**, associated with a characteristic broad feature in the DSC traces (see **Fig. S27 and S28**) and exists over temperature ranges of ~9 K and ~14 K for **C10/B10** and **C10/B12**, respectively. The Iso$_1^{[*]}$ phase of both complexes transforms into the chiral triple network Cub$_{bi}^{[*]}$/*I*23 phase on cooling. Because it appears adjacent to a Cub$_{bi}^{[*]}$/*I*23 phase it seems that this Iso$_1^{[*]}$ phase represents a distorted version of the *I*23 phase, retaining a long-range chirality synchronization due to a local *I*23-like network structure in the isotropic liquid state. Similar to **A6/B8** and **A10/B8** chirality could be also retained in the crystalline state (Cr$^{[*]}$) even after sample storage for several months (Table 2).

For the longest supramolecule **C10/B14** the Iso$_1^{[*]}$ phase is removed and replaced by a Col$_{hex}$ phase on cooling from the achiral isotropic liquid at ~*T* = 179 °C. It is a metastable phase for a short temperature range of ~6 K followed by Cub$_{bi}^{[*]}$/*I*23 at *T* = 173 °C which then transforms to a birefringent crystalline phase (Cr) at *T* = 89 °C (for XRD see Table S16-S18 and Fig. S18). Upon heating a Cub$_{bi}$/*Ia*$\bar{3}$*d*^{LT} phase is found (similar to complex **A10/B8**), which transforms at 150 °C into the Cub$_{bi}^{[*]}$/*I*23 phase on further heating.

3.3. Discussion of the self-assembly and mirror symmetry breaking in the Cub$_{bi}$ phases

The series **A*n*/B*m*** and **C*n*/B*m*** cover different and partly overlapping chain volume ranges (Σ = 26–44 and 20–34, respectively) which leads to different sections of a common phase sequence evolving in each of the series (see Figs. 2 and 7). The change of the substitution pattern of the benzoic acid does not modify the mesophase types and leads only to a slight shift of the distinct phase ranges with respect to Σ. Among the Cub$_{bi}$ phases there is obviously only one type of *I*23 phase and possibly three or even four subtypes of the *Ia*$\bar{3}$*d* phase. The *Ia*$\bar{3}$*d* phase occurring for complexes with Σ between 10 and 28 is replaced by the *I*23 phase upon increasing the alkyl chain volume (Σ = 26–44; Figs. 2b, 7b). Moreover, there is a re-entrance of the *Ia*$\bar{3}$*d* lattice for complexes with largest chain volume (Σ = 40–44). This sequence *Ia*$\bar{3}$*d* → *I*23 → *Ia*$\bar{3}$*d* was previously observed in several homologous series of polycatenar mesogens [42,49] and was attributed to an increasing helical twist between the molecules, which modifies the cubic space group and leads to two subtypes of *Ia*$\bar{3}$*d* phases, the long pitch and the short pitch phases [49–51,54]. However, in the series of H-bonded complexes reported here, there is no such clear trend of the helical pitch length (see Tables S6 and S19). Nevertheless, there are two distinct chain volume ranges of the *Ia*$\bar{3}$*d* phase. The *Ia*$\bar{3}$*d* phase of the high chain volume complexes occurs below *I*23 for **A10/B8** and **C10/B14** (Fig. 2a, 7a), but upon further chain elongation it becomes a high temperature phase above *I*23 which competes with the Col$_{hex}$ phase (*Ia*$\bar{3}$*d*^{HT}).

It appears that the type of *Iad* phase is not only a function of the helical twist, but also influenced by the changing interface curvature at the lamellar-columnar transition. The *Ia*$\bar{3}$*d*^{LT} phase seems to be stabilized by reduced chain expansion and therefore is more considered as being derived from a lamellar phase by curvature,

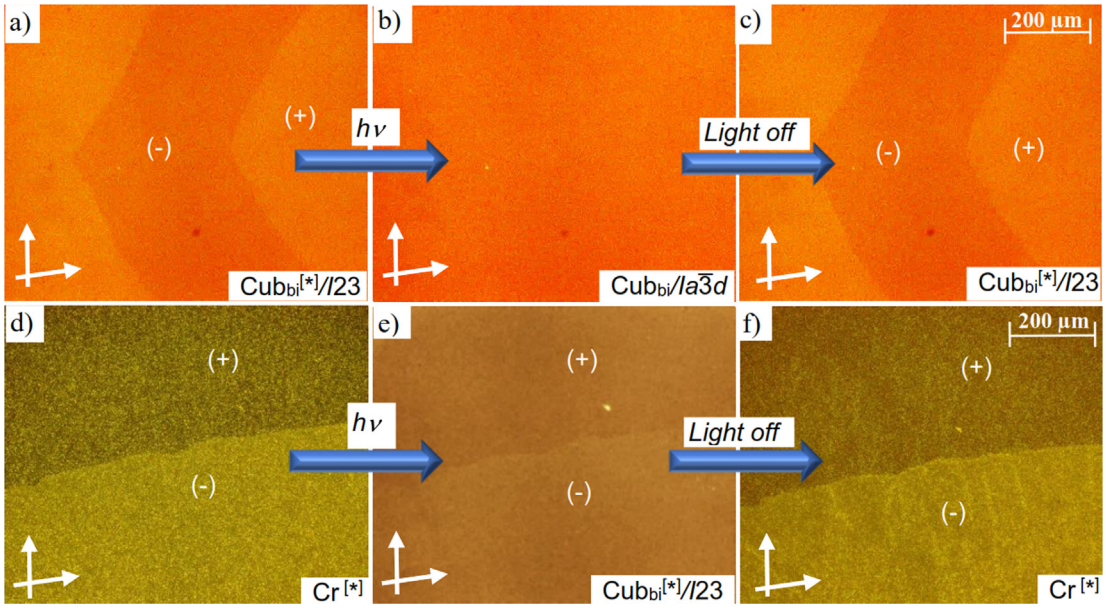

Fig. 10. (a-c) Reversible isothermal photo-off–on switching of chirality as observed for **A10/B8** in a homeotropic cell at T = 150 °C; (a) and (c) show chiral conglomerate textures of the chiral $I23$ phase, whereas the photoinduced achiral $Ia\bar{3}d$ phase in b) shows no such domains. (d-f) Switching between the $Cr^{[*]}$ and the $Cub_{bi}^{[*]}/I23$ phase by retaining chirality and conglomerate texture at T = 70°.

whereas the formation of the $Ia\bar{3}d^{HT}$ phase is associated with thermal alkyl chain expansion and thus is considered as more related to columnar self-assembly and fusion of these columns to networks. Moreover, it is hypothesized that the $Ia\bar{3}d^{HT}$ phase formed from the chiral $I23$ phase on heating (complexes **A10/B10** – **A10/B14**) retains its helical network structure and becomes a *meso*-structure, but if formed on cooling from the achiral isotropic liquid (**A10/B8**) the $Ia\bar{3}d^{HT}$ phase apparently evolves as a non-helical network phase, like those known for lyotropic systems and polymers and in this case only after transition to $I23$ a long range network helicity develops [40]. For complexes with longer chains this achiral $Ia\bar{3}d^{HT}$ phase is replaced by Col_{hex} on cooling. On heating the $Ia\bar{3}d^{HT}$ phase develops from the $I23$ phase and is retained as long as there is sufficient network connectivity and helix synchronization. The proposed overall picture of the development of the distinct cubic phases is sketched in Fig. 9.

3.4. Isothermal photo switching in mirror symmetry broken network phases

The incorporation of azo units into the structures of the newly reported supramolecules allows the possibility of studying photoisomerization under UV irradiation. All previously studied azobenzene-based polycatenars elucidated the possibility of photoswitching in solutions as well as between different fluid LC phases, which in most cases represent lamellar or nematic phases [64,65,83–87]. Only recently, successful isothermal light-induced transformation between SmC and Cub_{bi} phases was reported for binary mixtures of azobenzene molecules with 4′-*n*-alkoxy-3′-nitro biphenyl-4-carboxylic acid or 4′-*n*-hexadecyloxy-3′-cyanobiphenyl-4-carboxylic acid, but not for polycatenars [72,73,88]. A breakthrough came with the first report about the rapid and reversible photo switching between chiral $Iso^{[*]}$ and achiral lamellar SmA phases exhibited by azobenzene-based polycatenars.[62] The next issue to be addressed was to check the possibility to photo switch between chiral and achiral cubic phases (Fig. 1b,c). To the best of our knowledge, up to date there is no report about such transformation. The supramolecule **A10/B8** was selected for such investigations as a representative example. **A10/B8** was sandwiched between normal glass slides on a temperature controlled heating stage and irradiated firstly in the chiral $Cub_{bi}^{[*]}/I23$ phase at T = 150 °C, i.e. close to $Cub_{bi}^{[*]}/I23$- $Cub_{bi}/Ia\bar{3}d$ phase transition temperature, by UV light (365 nm). As obvious from Fig. 10a,b, the conglomerate texture disappears upon irradiation within < 3 s. This indicates that a fast isothermal transformation from the chiral to the achiral Cub_{bi} phase was achieved. The achiral $Cub_{bi}/Ia\bar{3}d$ phase relaxes back to the chiral domain texture of the $Cub_{bi}^{[*]}/I23$ phase almost immediately after switching off the light source (<3 s; see Fig. 10c). Therefore, this observation elucidates the first example of a fast and reversible photoswitching between a chiral and an achiral cubic LC mesophase.

Likewise, a photoinduced isothermal transition from the crystalline $Cr^{[*]}$ phase to the liquid crystalline $Cub_{bi}^{[*]}/I23$ phase at T = 70 °C was also achieved, which is also very fast and reversible (see Fig. 10d-f). The completely isotropic texture of $Cub_{bi}^{[*]}/I23$ phase relaxes back to the low birefringent texture of the $Cr^{[*]}$ phase after switching the light off. In both cases the chiral domains after switching off the light source are observed in the same regions with the same handedness as before light irradiation. This is attributed to the high viscosity due to the 3D lattice of the cubic phases and the storage of the chiral information at least at the interfaces to the glass substrates. These transitions are mainly due to a shift of the phase transition temperatures by photoisomerization. The bent shape of the photoinduced *cis*-isomer shifts the phase transitions $Cub_{bi}^{[*]}/I23$ - $Cub_{bi}/Ia\bar{3}d$ and $Cr^{[*]}$ - $Cub_{bi}^{[*]}/I23$ to lower temperatures. Therefore, the supramolecules reported herein represent the first examples of materials capable of photoswitching between chiral and achiral 3D networks by light irradiation. Moreover, it was also possible to photo-switch between crystalline and liquid crystalline phases.

4. Summary and conclusions

In summary, we reported the design, synthesis, and molecular self-assembly of new photosensitive nanostructured supramolecu-

lar azopyridine-based polycatenars formed by intermolecular hydrogen-bond between Y-shaped or taper shaped benzoic acids and linear azopyridine derivatives (Fig. 1a). The formation of mirror-symmetry broken $Cub_{bi}^{[*]}$ and $Iso_{I}^{[*]}$ phases was successfully controlled by alkyl-chain engineering via changing the number and positions as well as the length of terminal alkyl chains at both ends of the supramolecules (Figs. 2 and 7). Chirality synchronization by helical network formation was observed in the triple network cubic phase with *I*23 symmetry as well as in the isotropic liquid phase ($Iso_{I}^{[*]}$). The $Iso_{I}^{[*]}$ phase is observed only adjacent to the *I*23 cubic phase, which means that it is likely to have a local *I*23-like structure. In addition to these chiral phases achiral cubic phases with $Ia\bar{3}d$ symmetry as well as a Col_{hex} phases are observed depending on the length of the terminal alkyl chains (Fig. 9). Moreover, the synthesized supramolecules represent the first examples of fast and reversible photo switching by UV irradiation between $Cub_{bi}^{[*]}$/*I*23 and Cub_{bi}/$Ia\bar{3}d$ phases. This could lead to interesting perspectives for chirality switching and phase modulation by interaction with non-polarized light [71], which in turn could be used to improve the materials properties to be applied in optical shutters and other optical, electronic, or mechanical modulation devices.

CRediT authorship contribution statement

M. Alaasar: Conceptualization, Investigation, Data curation, Supervision, Methodology, Writing-original draft, Writing-review and editing. **X. Cai:** Investigation, Methodology, Data curation, Software. **F. Kraus:** Investigation, Methodology. **M. Giese:** Writing-review and editing. **F. Liu:** Data curation, Software, Supervision, Writing-review and editing. **C. Tschierske:** Writing-review and editing, Supervision.

Declaration of Competing Interest

The authors declare that they have no known competing financial interests or personal relationships that could have appeared to influence the work reported in this paper.

Acknowledgements

M. Alaasar acknowledges the German Research Foundation (DFG) for the financial support (AL2378/1-1, 424355983). F. Liu thanks Science and Technology Agency of Shaanxi Province (2016KW-050 and 2018KWZ-03) for the financial support. The authors are grateful to Beamline BL16B1 at SSRF (Shanghai Synchrotron Radiation Facility, China) for providing the beamtime.

Appendix A. Supplementary material

Supplementary data to this article can be found online at https://doi.org/10.1016/j.molliq.2022.118597.

References

[1] H. Takezoe, Spontaneous achiral symmetry breaking in liquid crystalline phases, in: C. Tschierske (Ed.), Liquid Crystals, Topics in Current Chemistry; Springer, Berlin, Vol. 318, 2011, pp 303−330.
[2] C. Tschierske, Liq. Cryst. 45 (2018) 2221.
[3] C. Tschierske, G. Ungar, ChemPhysChem. 17 (2016) 1224.
[4] T. Sekine, T. Niori, J. Watanabe, T. Furukawa, S.-W. Choi, H. Takezoe, J. Mater. Chem. 7 (1997) 1307.
[5] L.E. Hough, H.T. Jung, D. Kruerke, M.S. Heberling, M. Nakata, C.D. Jones, D. Chen, D.R. Link, J. Zasadzinski, G. Heppke, J.P. Rabe, W. Stocker, E. Korblova, D.M. Walba, M.A. Glaser, N.A. Clark, Science 325 (2009) 456.
[6] C. Zhang, N. Diorio, O.D. Lavrentovich, A. Jákli, Nat. Commun. 5 (2014) 3302.
[7] K.V. Le, H. Takezoe, F. Araoka, Adv. Mater. 29 (2017) 1602737.
[8] M. Alaasar, M. Prehm, M. Brautzsch, C. Tschierske, J. Mater. Chem. C. 2 (2014) 5487.
[9] M. Alaasar, M. Prehm, C. Tschierske, Chem. Eur. J. 22 (2016) 6583.
[10] A. Lehmann, M. Alaasar, M. Poppe, S. Poppe, M. Prehm, M. Nagaraj, S.P. Sreenilayam, Y.P. Panarin, J.K. Vij, C. Tschierske, Chem. – Eur. J. 26 (2020) 4714.
[11] M. Poppe, M. Alaasar, A. Lehmann, S. Poppe, M.G. Tamba, J.K. Vij, M. Kurachkina, X. Cai, F. Liu, A. Eremin, M. Nagaraj, C. Tschierske, J. Mater. Chem. C. 8 (2020) 3316.
[12] M. Alaasar, M. Prehm, M. Nagaraj, J.K. Vij, C. Tschierske, Adv. Mater. 25 (2013) 2186.
[13] M. Alaasar, M. Prehm, S. Belau, N. Sebastián, M. Kurachkina, A. Eremin, C. Chen, F. Liu, C. Tschierske, Chem. Eur. J. 25 (2019) 6362.
[14] M. Nagaraj, Liq. Cryst. 43 (2016) 2244.
[15] R.J. Mandle, Chem. Eur. J. 23 (2017) 8771.
[16] J.P. Abberley, R. Killah, R. Walker, J.M.D. Storey, C.T. Imrie, M. Salamończyk, C. Zhu, E. Gorecka, D. Pociecha, Nat. Commun. 9 (2018) 228.
[17] T. Kato, J. Uchida, T. Ichikawa, T. Sakamoto, Angew. Chem. Int. Ed. 57 (2018) 4355.
[18] Q. Li (Ed.), Nanoscience with Liquid Crystals, Springer, Cham, 2014.
[19] N. Koide (Ed.), The Liquid Crystal Display Story, Springer Japan, Tokyo, 2014.
[20] C.M. Paleos, D. Tsiourvas, Liq. Cryst. 28 (2001) 1127.
[21] X.-H. Cheng, H.-F. Gao, Hydrogen bonding for supramolecular liquid crystals, in: Z.-T. Li, L.-Z. Wu (Eds.), Hydrogen Bonded Supramolecular Materials, Lecture Notes in Chemistry, vol. 88, no. 5, 2015, pp. 133–183 (Chapter 5). https://doi.org/10.1007/978-3-662-45780-1.
[22] H.K. Bisoyi, Q. Li, Angew. Chem. Int. Ed. 55 (2016) 2994.
[23] D.W. Bruce, Liquid crystals formed from specific intermolecular interactions, in: P.A. Gale, J.W. Steed (Eds.), Supramolecular Chemistry: From Molecules to Nanomaterials, Wiley, vol. 7, , 2012, pp. 3493–3514.
[24] M. Saccone, L. Catalano, J. Phys. Chem. B. 123 (2019) 9281.
[25] T. Kato, J.M.J. Frechet, Macromolecules 22 (1989) 3818.
[26] S.K. Kang, E.T. Samulski, Liq. Cryst. 27 (2000) 371.
[27] S.K. Kang, E.T. Samulski, P. Kang, J. Choo, Liq. Cryst. 27 (2000) 377.
[28] C. Tschierske, Angew. Chem. Int. Ed. 52 (2013) 8828.
[29] T. Kato, in: J.W. Goodby, P.J. Collings, T. Kato, C. Tschierske, H. Gleeson, P. Raynes, (Eds.), Handbook of Liquid Crystals, Wiley-VCH, Weinheim, vol. 6, Nanoparticle and Nanostructured Liquid Crystals, 2014.
[30] R. Zhang, Z. Su, X.-Y. Yan, J. Huang, W. Shan, X.-H. Dong, X. Feng, Z. Lin, S.Z.D. Cheng, Chem. Eur. J. 26 (2020) 6741.
[31] R. Walker, D. Pociecha, J.P. Abberley, A. Martinez-Felipe, D.A. Paterson, E. Forsyth, G.B. Lawrence, P.A. Henderson, J.M.D. Storey, E. Gorecka, C.T. Imrie, Chem. Commun. 54 (2018) 3383.
[32] R. Walker, D. Pociecha, A. Martinez-Felipe, J.M.D. Storey, E. Gorecka, C.T. Imrie, Crystals 10 (2020) 175.
[33] S. Bujosa, E.E. Greciano, M.A. Martínez, L. Sánchez, B. Soberats, Chem. Eur. J. (2021), https://doi.org/10.1002/chem.202102446.
[34] G.W. Gray, B. Jones, F. Marson, J. Chem. Soc. (1957) 393.
[35] Y. Yamamura, Y. Nakazawa, S. Kutsumizu, K. Saito, Phys. Chem. Chem. Phys. 21 (2019) 23705.
[36] M. Imperor-Clerc, M. Veber, A.M. Levelut, Chem. Phys. Chem. 8/9 (2001) 533.
[37] M. Imperor-Clerc, P. Sotta, M. Veber, Liq. Cryst. 27 (2000) 1001.
[38] X. Zeng, G. Ungar, M. Imperor-Clerc, Nat. Mater. 4 (2005) 562.
[39] A. Kohlmeier, D. Janietz, S. Diele, Chem. Mater. 18 (2006) 1483.
[40] Y. Cao, M. Alaasar, A. Nallapaneni, M. Salamończyk, P. Marinko, E. Gorecka, C. Tschierske, F. Liu, N. Vaupotič, C. Zhu, Phy. Rev. lett. 125 (2020) 027801.
[41] T. Kato, M. Yoshio, T. Ichikawa, B. Soberats, H. Ohno, M. Funahashi, Nat. Rev. Mater. 2 (2017) 17001.
[42] S. Kutsumizu, Isr. J. Chem. 52 (2012) 844.
[43] O. Kwon, X. Cai, W. Qu, F. Liu, J. Szydlowska, E. Gorecka, M.J. Han, D.K. Yoon, S. Poppe, C. Tschierske, Adv. Funct. Mater. 31 (2021) 2102271.
[44] M. Alaasar, A.F. Darweesh, X. Cai, F. Liu, C. Tschierske, Chem. Eur. J. 24 (2021) 14921.
[45] H.T. Nguyen, C. Destrade, J. Malthete, Adv. Mater. 9 (1997) 375.
[46] W. Weissflog, in: J.W. Goodby, J.P. Collings, T. Kato, C. Tschierske, H.F. Gleeson, P. Raynes (Eds.), Handbook of Liquid Crystals, Wiley-VCH, Weinheim, second ed., vol. 5, 2014, pp. 89–174.
[47] C. Dressel, F. Liu, M. Prehm, X. Zeng, G. Ungar, C. Tschierske, Angew. Chem. Int. Ed. 53 (2014) 13115.
[48] C. Dressel, T. Reppe, M. Prehm, M. Brautzsch, C. Tschierske, Nat. Chem. 6 (2014) 971.
[49] T. Reppe, C. Dressel, S. Poppe, C. Tschierske, Chem. Commun. 56 (2020) 711.
[50] C. Dressel, T. Reppe, S. Poppe, M. Prehm, X. Lu, G. Zeng, C.T. Ungar, Adv. Funct. Mater. 2004353 (2020).
[51] T. Reppe, S. Poppe, X. Cai, Y. Cao, F. Liu, C. Tschierske, Chem, Sci. 11 (2020) 5902.
[52] T. Reppe, S. Poppe, C. Tschierske, Chem. Eur. J. 26 (2020) 16066.
[53] M. Alaasar, S. Poppe, Y. Cao, C. Chen, F. Liu, C. Zhu, C. Tschierske, J. Mater. Chem. C 8 (2020) 12902.
[54] X. Zeng, G. Ungar, J. Mater. Chem. C. 8 (2020) 5389.
[55] H. Yu, T. Ikeda, Adv. Mater. 23 (2011) 2149.
[56] Z. Mahimwalla, K.G. Yager, J.-I. Mamiya, A. Shishido, A. Priimagi, C.J. Barrett, Polym. Bull. 69 (2012) 967.
[57] L. De Sio, N. Tabiryan, T. Bunning, B.R. Kimball, C. Umeton, Chapter 1 – Dynamic photonic materials based on liquid crystals, in: E. Wolf (Ed.), Progress in Optics, Elsevier, Amsterdam, vol. 58, , 2013, pp. 1–64.
[58] M. Alaasar, Liq. Cryst. 43 (2016) 2208.

[59] M. Saccone, M. Spengler, M. Pfletscher, K. Kuntze, M. Virkki, C. Wölper, R. Gehrke, G. Jansen, P. Metrangolo, A. Priimagi, M. Giese, Chem. Mater. 31 (2019) 462.
[60] M. Pfletscher, C. Wölper, J.S. Gutmann, M. Mezger, M. Giese, Chem. Commun. 52 (2016) 8549.
[61] M. Alaasar, M. Prehm, Y. Cao, F. Liu, C. Tschierske, Angew. Chem. Int. Ed. 128 (2016) 320.
[62] M. Alaasar, S. Poppe, Q. Dong, F. Liu, C. Tschierske, Angew. Chem., Int. Ed. 56 (2017) 10801.
[63] M. Alaasar, M. Prehm, S. Belau, N. Sebastian, M. Kurachkina, A. Eremin, C. Chen, F. Liu, C. Tschierske, Chem. Eur. J. 25 (2019) 6362.
[64] M. Alaasar, S. Poppe, Liq. Cryst. 47 (2020) 939.
[65] J.M. Shivanna, M. Alaasar, G. Hegde, J. Mol. Liq. 341 (2021) 117341.
[66] H.M.D. Bandara, S.C. Burdette, Chem. Soc. Rev. 2012 (1809) 41.
[67] H.K. Bisoyi, Q. Li, Acc. Chem. Res. 47 (2014) 3184.
[68] J.-I. Mamiya, K. Kanie, T. Hiyama, T. Ikeda, T. Kato, Chem. Commun. (2002) 1870.
[69] Z.-G. Zheng, Y.-Q. Lu, Q. Li, Adv. Mater. (2020) 1905318.
[70] H.K. Bisoyi, T.J. Bunning, Q. Li, Adv. Mater. 30 (2018) 1706512.
[71] D.A. Paterson, J. Xiang, G. Singh, R. Walker, D.M. Agra-Kooijman, A. Martınez-Felipe, M. Gao, J.M.D. Storey, S. Kumar, O.D. Lavrentovich, C.T. Imrie, J. Am. Chem. Soc. 138 (2016) 5283.
[72] R. Hori, Y. Miwa, K. Yamamoto, S. Kutsumizu, J. Phys. Chem. B 118 (2014) 3743.
[73] A. Nagai, H. Kondo, Y. Miwa, T. Kondo, S. Kutsumizu, Y. Yamamura, K. Saito, Bull. Chem. Soc. Jpn. 91 (2018) 1652.
[74] M. Alaasar, S. Poppe, Q. Dong, F. Liu, C. Tschierske, Chem. Commun. 52 (2016) 13869.
[75] M. Alaasar, S. Poppe, C. Tschierske, J. Mol. Liq. 277 (2019) 233.
[76] M. Alaasar, J.C. Schmidt, X. Cai, F. Liu, C. Tschierske, J. Mol. Liq. 332 (2021) 115870.
[77] M. Lehmann, M. Dechant, M. Lambov, T. Ghosh, Acc. Chem. Res. 52 (2019) 1653.
[78] E.J. Foster, R.B. Jones, C. Lavigueur, V.E. Williams, J. Am. Chem. Soc. 128 (2006) 8569.
[79] E. Beltrán, J.L. Serrano, T. Sierra, R. Giménez, J. Mater. Chem. 22 (2012) 7797.
[80] P. Staffeld, M. Kaller, S.J. Beardsworth, K. Tremel, S. Ludwigs, S. Laschat, F. Giesselmann, J. Mater. Chem. C 1 (2013) 892.
[81] Y.J. Chen, H.F. Yu, L.Y. Zhang, H. Yang, Y.F. Lu, Chem. Commun. 50 (2014) 9647.
[82] Y. Cao, C. Feng, A. Jakli, C. Zhu, F. Liu, Giant 2 (2020) 100018.
[83] H. Chen, R. Zhang, H. Gao, H. Cheng, H. Fang, X. Cheng, Dyes Pigments 149 (2018) 512.
[84] X. Peng, H. Gao, Y. Xiao, H. Cheng, F. Huang, X. Cheng, N. J. Chem. 2017 (2004) 41.
[85] R. Yamakado, M. Hara, S. Nagano, T. Seki, H. Maeda, Chem.-Eur. J. 23 (2017) 9244.
[86] V. Prasad, S.-W. Kang, S.K. Varshney, N.G. Nagaveni, Liq. Cryst. 37 (2010) 121.
[87] N.G. Nagaveni, M. Gupta, A. Roy, V. Prasad, J. Mater. Chem. 20 (2010) 9089.
[88] R. Hori, D. Furukawa, K. Yamamoto, S. Kutsumizu, Chem. Eur. J. 18 (2012) 7346.